Inorg. Chem. **2009**, *48*, 3371−3381

Forum

Spin-Crossover Behavior in Cyanide-Bridged Iron(II)−Copper(I) Bimetallic 1−3D Metal−Organic Frameworks

Gloria Agustí,[†] M. Carmen Muñoz,[‡] Ana B. Gaspar,[†] and José A. Real*[,†]

Institut de Ciència Molecular, Departament de Química Inorgànica, Universitat de València, Edifici d'Instituts de Paterna, P.O. Box 22085, 46071 València, Spain, and Departament de Física Aplicada, Universitat Politècnica de València, Camí de Vera s/n, 46022 València, Spain

Received June 10, 2008

The synthesis and characterization of a series of 1−3D cyanide-bridged iron(II)−copper(I) bimetallic coordination polymers formulated as $\{Fe(3\text{-}Xpy)_2[Cu(3\text{-}Xpy)_z(CN)_2]_2\}$, where 3-Xpy is a 3-halogenpyridine ligand with X = F (z = 1.5, **1**), Cl (z = 1, **2** and **3**), Br (z = 1, **4**), and I (z = 1, **5**), are reported. In all derivatives, the Fe^{II} ion lies in pseudooctahedral $[FeN_6]$ sites defined by four in situ formed $[Cu(3\text{-}Xpy)_z(CN)_2]^-$ bridging ligands and two 3-Xpy terminal ligands occupying the equatorial and axial positions, respectively. **1** consists of stacks of corrugated grids whose square windows are defined by pseudotrigonal and pseudotetrahedral $[Cu(3\text{-}Fpy)(CN)_2]^-$ and $[Cu(3\text{-}Fpy)_2(CN)_2]^-$ units, respectively. **2** is a 3D coordination polymer with the topology of the open-framework $CdSO_4$. The $[Cu(3\text{-}Clpy)(CN)_2]^-$ rods connecting the pseudooctahedral Fe^{II} sites are arranged in such a way that interpenetration is avoided. **3**, an architectural isomer of **2**, is defined by arrays of linear chains. **4** and **5** are isostructural to **3**. Polymer **1** is essentially a low-spin (LS) compound with ca. 19% of residual Fe^{II} ions in the high-spin (HS) state at 293 K. It undergoes an irreversible spin transition at T_c = 356 K. Subsequent cooling−warming cycles give a new spin-crossover behavior characterized by T_c = 187 K. The structural analysis at 130 and 293 K and at 293 K after irreversible transformation (293 K*) reveals a large unit cell volume variation of 67 Å^3 per Fe atom. In addition to the volume change associated with the spin-state conversion, remarkable bond and angle modifications around the Cu^I sites account for the high flexible nature of the crystal. **2** displays a complete not well-resolved two-step spin conversion, T_{c1} = 169 K and T_{c2} = 210 K, reflecting the occurrence of two distinct crystallographically Fe^{II} sites. The large unit cell volume variation per Fe atom in **2**, 59 Å^3, has been rationalized in terms similar to those for **1**. 1D polymers **3**−**5** are HS compounds.

Introduction

The synthesis of spin-crossover (SCO) compounds displaying strong cooperative first-order spin transitions with large thermal hysteresis near room temperature is a current challenge in coordination chemistry.[1] Such attractive bistable compounds could ultimately be useful for the construction of memory and sensory molecular-based devices.[2] Cooperativity depends on how efficiently the structural characteristics associated with each spin state are transmitted to the whole crystal during the low-spin (LS) ↔ high-spin (HS) transformation. This fact has stimulated the search for new synthetic strategies directed to improve connectivity between Fe^{II} SCO centers, thereby obtaining more rigid networks able to transmit effectively the spin-state change.[3]In this respect, the possibility of inducing polymerization through suitable cyanometalate bridging ligands was considered relatively recently in the SCO area. Kitazawa and co-workers synthesized the first cyanide-bridged SCO coordination 2D polymer

* To whom correspondence should be addressed. E-mail: jose.a.real@uv.es.
[†] Universitat de València.
[‡] Universitat Politècnica de València.

(1) Gütlich, P., Goodwin, H. A., Eds. Spin Crossover in Transition Metal Compounds. *Topics in Current Chemistry*; Springer: New York, 2004; Vols. *233*, *234*, and *235*.

10.1021/ic8010458 CCC: $40.75
Published on Web 04/13/2009

{Fe(pyridine)$_2$[Ni(CN)$_4$]}.[4] Later on, Real and co-workers reported the isostructural $[Pd(CN)_4]^{2-}$ and $[Pt(CN)_4]^{2-}$ SCO derivatives and the 3D system {Fe(pyrazine)[M^{II}(CN)$_4$]} (M^{II} = Ni, Pd, and Pt),[5] which display hysteresis loops ca. 25 K wide containing room temperature when conveniently treated.[6] It has been demonstrated recently that the spin change in the Pt derivative can be triggered within the bistable region using a pulsed laser around room temperature[7] and that it can be grown as thin films on gold surfaces without losing essentially its properties.[8] More recently, cooperative spin transitions have also been reported for the 2D polymers {Fe(5-bromopyrimidine)$_2$[M^{II}(CN)$_4$]} (M^{II} = Ni, Pd, and Pt) with critical temperatures in the temperature range 170−225 K.[9] All of these compounds display a marked change of color upon spin conversion. On the basis of the results above, we started a systematic study that also included the cyanometalate bridging ligands $[M^I(CN)_2]^-$ (M^I = Cu, Ag, and Au). The $[M^I(CN)_2]^-$ building blocks have afforded a number of singular 1−3D structures with a rich variety of topologies and interesting properties. For instance, the systems {Fe(L)$_x$[M^I(CN)$_2$]$_2$}·nG [M^I = Ag; L = pyrazine (x = 1, nG = 1 pyrazine), 4,4′-bipyridine (x = 2), and bis(pyridylethylene) (x = 2)] are doubly interpenetrated 3D polymers.[10] The former is LS at 300 K, while the other two complexes display strong cooperative spin transitions. Triply interpenetrated 3D SCO networks with NbO topology have also been reported for {Fe(3-cyanopyridine)$_2$[M^I(CN)$_2$]$_2$}·nH$_2$O (M^I = Ag or Au and n = $^2/_3$).[11] Significant metallophilic interactions [3.256(2)−3.1593(6) and 3.4212(13)−3.3952(17) Å for silver and gold derivatives, respectively] occur between consecutive networks for both derivatives. Interestingly, the Ag···Ag interactions strongly depend on the spin state of the Fe^{II} atoms displaying a variation of ca. 0.1 Å, which results in an abnormally large variation of the unit cell volume. When the organic ligand L is pyrimidine, a singular family of coordination SCO polymers was obtained. The {Fe(pmd)(H$_2$O)[M^I(CN)$_2$]$_2$}·H$_2$O (M^I = Ag and Au) coordination polymers, constituted of triply interpenetrated 3D frameworks, undergo cooperative spin transitions with thermal hysteresis (ca. 8 K) as well as a singular reversible ligand-exchange reaction in the solid state involving coordinated water and pyrimidine ligands, giving the 3D polymers {Fe(pmd)[M^I(CN)$_2$]$_2$} (M^I = Ag and Au), which display different magnetic behavior.[12] Pressure-tuneable thermal hysteresis and a piezohysteresis loop at room temperature on the silver derivative have been demonstrated from its magnetic and optical properties. Pressure allows one to tune the hysteresis width and to place the hysteresis loop at will in a large range of temperatures, including room temperature, without losing its well-defined square shape.[13] Three additional silver(I) polymers were isolated, two of which are architectural isomers of {Fe(pmd)$_2$[Ag(CN)$_2$]$_2$}[14] and {Fe(pmd)[Ag(CN)$_2$][Ag$_2$(CN)$_3$]}.[15] The latter shows a rather complicated self-interpenetrated 3D structure with strong Ag···Ag contacts [3.286(2)−2.934(3) Å] dependent on the spin state and a singular thermo- and photoinduced two-step spin transition. More recently, a new series of complexes {Fe(3-Xpy)$_2$[M(CN)$_2$]$_2$} (M^I = Ag[16] and Au[17]) based on 3-halogenpyridine ligands (3-Xpy; X = F, Cl, Br, and I) was undertaken. Silver and gold derivatives display similar structures made up of the stacking of pairs of slightly corrugated 2D polymeric networks. The pairs of layers are held together by strong metallophilic interactions [3.2727(11)−2.9635(11) and 3.580(8)−3.0137(8) Å for silver and gold derivatives, respectively]. These crystalline materials are fully HS at 300 K. However, in the $[Ag(CN)_2]^-$ polymers, the 3-Fpy and 3-Clpy derivatives undergo thermally induced two-step and half-spin transitions, respectively, while only the 3-Fpy polymer displays a half-spin transition in the gold derivatives. As usual, the spin transition in these compounds is coupled with a marked color change from pale yellow in the HS state to deep red in the LS state. Interestingly, the silver derivatives afford a second type of red-colored crystalline materials in the presence of an excess of 3-Brpy or 3-Ipy where the LS state is strongly stabilized at 300 K. In these clathrate materials, two additional 3-Xpy molecules are included in the framework, one is coordinated to a $[Ag(CN)_2]^-$ anion and the other one remains as an uncoordinated guest molecule, thereby inducing dissociation of the double layers and, consequently, breaking the argentophilic interactions. Inclusion of an uncoordinated 3-Ipy guest molecule in the Fe^{II}-3-Ipy-$[Au(CN)_2]^-$ system also afforded

(2) (a) Real, J. A.; Gaspar, A. B.; Muñoz, M. C. *Dalton Trans.* **2005**, 2062. (b) Gaspar, A. B.; Ksenofontov, V.; Seredyuk, M.; Gütlich, P. *Coord. Chem. Rev.* **2005**, *249*, 2661. (c) Real, J. A.; Gaspar, A. B.; Niel, V.; Muñoz, M. C. *Coord. Chem. Rev.* **2003**, *236*, 121. (d) Bousseksou, A.; Molnár, G.; Matouzenko, G. *Eur. J. Inorg. Chem.* **2004**, 4353.

(3) (a) Vreugdenhil, W.; van Diemen, J. H.; De Graaff, R. A. G.; Haasnoot, J. G.; Reedijk, J.; Kahn, O.; Zarembowitch, J. *Polyhedron* **1990**, *9*, 2971. (b) Real, J. A.; Andrés, E.; Muñoz, M. C.; Julve, M.; Granier, T.; Bousseksou, A.; Varret, F. *Science* **1995**, *268*, 265. (c) Kahn, O.; Martinez, J. C. *Science* **1998**, *279*, 44. (d) Garcia, Y.; Kahn, O.; Rabardel, L.; Chansou, B.; Salmon, L.; Tuchagues, J. P. *Inorg. Chem.* **1999**, *38*, 4663. (e) Halder, G. J.; Kepert, C. J.; Moubaraki, B.; Murray, K. S.; Cashion, J. D. *Science* **2002**, *298*, 1762. (f) Garcia, Y.; Niel, V.; Real, J. A. *Top. Curr. Chem.* **2004**, *233*, 229.

(4) Kitazawa, T.; Gomi, Y.; Takahashi, M.; Takeda, M.; Enemoto, A.; Miyazaki, T.; Enoki, T. *J. Mater. Chem.* **1996**, *6*, 119.

(5) Niel, V.; Martinez-Agudo, J. M.; Muñoz, M. C.; Gaspar, A. B.; Real, J. A. *Inorg. Chem.* **2001**, *40*, 3838.

(6) Tayagaki, T.; Galet, A.; Molnár, G.; Muñoz, M. C.; Zwick, A.; Tanaka, K.; Real, J. A.; Bousseksou, A. *J. Phys. Chem. B* **2005**, *109*, 14859.

(7) Bonhommeau, S.; Molnár, G.; Galet, A.; Zwick, A.; Real, J. A.; McGarvey, J. J.; Bousseksou, A. *Angew. Chem., Int. Ed.* **2005**, *44*, 4069.

(8) (a) Cobo, S.; Molnár, G.; Real, J. A.; Bousseksou, A. *Angew. Chem., Int. Ed.* **2006**, *45*, 5786. (b) Molnár, G.; Cobo, S.; Real, J. A.; Carcenac, F.; Daran, E.; Vieu, C.; Bousseksou, A. *Adv. Mater.* **2007**, *19*, 2163.

(9) Agustí, G.; Gaspar, A. B.; Muñoz, M. C.; Real, J. A. *Inorg. Chem.* **2007**, *46*, 9646.

(10) Niel, V.; Muñoz, M. C.; Gaspar, A. B.; Galet, A.; Levchenko, G.; Real, J. A. *Chem.—Eur. J.* **2002**, *8*, 2446.

(11) (a) Galet, A.; Niel, V.; Muñoz, M. C.; Real, J. A. *J. Am. Chem. Soc.* **2003**, *125*, 14224. (b) Galet, A.; Muñoz, M. C.; Martínez, V.; Real, J. A. *Chem. Commun.* **2004**, 2268.

(12) Niel, V.; Thompson, A. L.; Galet, A.; Muñoz, M. C.; Goeta, A. E.; Real, J. A. *Angew. Chem., Int. Ed.* **2003**, *42*, 3760.

(13) Galet, A.; Gaspar, A. B.; Muñoz, M. C.; Bukin, G. V.; Levchenko, G.; Real, J. A. *Adv. Mater.* **2005**, *17*, 2949.

(14) Galet, A.; Muñoz, M. C.; Gaspar, A. B.; Real, J. A. *Inorg. Chem.* **2005**, *44*, 8749.

(15) Niel, V.; Thompson, A. L.; Goeta, A. E.; Enachescu, C.; Hauser, A.; Galet, A.; Muñoz, M. C.; Real, J. A. *Chem.—Eur. J.* **2005**, *11*, 2047.

(16) Muñoz, M. C.; Gaspar, A. B.; Galet, A.; Real, J. A. *Inorg. Chem.* **2007**, *46*, 8182.

(17) Agustí, G.; Muñoz, M. C.; Gaspar, A. B.; Real, J. A. *Inorg. Chem.* **2008**, *47*, 2552.

a clathrate compound; however, in this case the aurophilic interactions persisted because they are stronger than the argentophilic interactions. So far, only two SCO coordination polymers containing the $[Cu(CN)_2]^-$ building block have been reported, namely, $\{Fe(pyrimidine)_2[Cu(CN)_2]_2\}$[18] and $\{Fe(3\text{-cyanopyridine})_2[Cu(3\text{-cyanopyridine})(CN)_2]_2\}$.[19] The former, a 2D polymer, undergoes thermo- and photoinduced cooperative spin transitions, while the latter, a 1D polymer, displays a continuous spin conversion. Aiming at completing the study of polymer compounds derived from $[M(CN)_2]^-$ and 3-Xpy and exploring new copper(I)−iron(II) bimetallic SCO complexes, here we report the synthesis and characterization of a new series of iron(II) SCO coordination polymers made up of $[Cu(CN)_2]^-$ and 3-Xpy (X = F, Cl, Br, and I) moieties. In contrast to the structural uniformity found in the silver(I) and gold(I) series, the $[Cu(CN)_2]^-$ anion affords $\{Fe(3\text{-Fpy})_2[Cu(3\text{-Fpy})_{1.5}(CN)_2]_2\}$ (**1**), a 2D SCO polymer, $\{Fe(3\text{-Clpy})_2[Cu(3\text{-Clpy})(CN)_2]_2\}$ (**2**), the only 3D $[Cu(CN)_2]^-$-based SCO system reported up to now, and the isostructural 1D coordination polymers $\{Fe(3\text{-Xpy})_2[Cu(3\text{-Xpy})(CN)_2]_2\}$ [X = Cl (**3**), Br (**4**), and I (**5**)]. Compounds **2** and **3** constitute an interesting example of architectural isomerism.

Experimental Section

Materials. $FeCl_2 \cdot 4H_2O$, 3-Xpy (X = F, Cl, Br, and I), $CuCl_2 \cdot 2H_2O$, and KCN were purchased from commercial sources and used as received. $K[Cu(CN)_2]$ was prepared by the addition of an aqueous solution containing an excess of KCN to a solution of $CuCl_2 \cdot 2H_2O$. Beige-colored crystals of $K[Cu(CN)_2]$ were grown after slow evaporation of the resulting solution. The crystalline bulk material was recrystallized twice before use.

Preparation of 1−5. Compounds **1**−**5** were synthesized by slow diffusion in 10 mL H-shaped vessels. A methanol−water (1:1) solution (2 mL) containing a mixture of $FeCl_2 \cdot 4H_2O$ (0.25 mmol, 49.7 mg) and 3-Xpy (1 mmol, 97.09 mg (X = F), 113.54 mg (X = Cl), 158 mg (X = Br) and 205 mg (X = I)) was poured in one side of the H-shaped vessel. The other side contained a methanol−water (1:1) solution (2 mL) of $K[Cu(CN)_2]$ (0.5 mmol, 77.34 mg). Then, the vessel was filled with a methanol−water (1:1) solution. Single crystals of **1**−**5** were formed over a period of 4 weeks. All of the manipulations were performed under an argon atmosphere. Anal. Calcd for $C_{29}H_{20}N_9F_5Cu_2Fe$ (**1**) (red): C, 45.09; H, 2.61; N, 16.32. Found: C, 44.89; H, 2.57; N, 16.19 (yield ca. 35%). Anal. Calcd for $C_{24}H_{16}N_8Cl_4Cu_2Fe$ (**2**) (red): C, 38.89; H, 2.18; N, 15.12. Found: C, 38.59; H, 2.21; N, 14.98 (yield ca. 30%). Anal. Calcd for $C_{24}H_{16}N_8Cl_4Cu_2Fe$ (**3**) (yellow): C, 38.89; H, 2.18; N, 15.12. Found: C, 38.31; H, 2.15; N, 15.05 (yield ca. 35%). Anal. Calcd for $C_{24}H_{16}N_8Br_4Cu_2Fe$ (**4**) (yellow): C, 31.37; H, 1.75; N, 12.19. Found: C, 31.43; H, 1.78; N, 12.05 (yield ca. 25%). Anal. Calcd for $C_{24}H_{16}N_8I_4Cu_2Fe$ (**5**) (yellow): C, 26.04; H, 1.46; N, 10.12. Found: C, 26.13; H, 1.48; N, 9.96 (yield ca. 25%). Crystals of **2** and **3** grow simultaneously in the H tube; they have been separated using a binocular lens because they have different shape and color.

Magnetic Measurements. The variable-temperature magnetic susceptibility measurements were carried out on samples constituted by small crystals (15−20 mg) using a Quantum Design MPMS2 SQUID susceptometer equipped with a 5.5 T magnet and operating at 1 T and 1.8−400 K. The susceptometer was calibrated with $(NH_4)_2Mn(SO_4)_2 \cdot 12H_2O$. Experimental susceptibilities were corrected for diamagnetism of the constituent atoms by the use of Pascal's constants.

Table 1. Crystal Data for **1**[a]

	293 K	130 K	293 K*
empirical formula	$C_{29}H_{20}N_9F_5Cu_2Fe$		
M_r	772.47		
cryst syst	monoclinic		
space group	$P2_1/c$		
a (Å)	17.1490(4)	17.0160(6)	17.2960(5)
b (Å)	12.7240(3)	12.6500(5)	13.0270(6)
c (Å)	13.6410(6)	13.5160(8)	13.8180(9)
β (deg)	91.6560(10)	91.532(2)	92.1810(10)
V (Å^3)	2975.28(16)	2908.3(2)	3111.1(3)
Z	4		
D_c (mg cm^{-3})	1.725	1.764	1.649
$F(000)$	1544		
μ(Mo Kα) (mm^{-1})	1.967	2.012	1.881
cryst size (mm)	0.04 × 0.08 × 0.08		
no. of total reflns	6795	6307	6156
no. of reflns [$I > 2\sigma(I)$]	4264	3139	2203
R1 [$I > 2\sigma(I)$]	0.0549	0.0875	0.0750
wR [$I > 2\sigma(I)$]	0.1430	0.1891	0.1201
S	0.970	0.989	0.921

[a] 293 K* stands for the crystal structure of **1** at 293 K after irreversible spin transition above 330 K. $R1 = \sum||F_o| - |F_c||/\sum|F_o|$; $wR = [\sum[w(F_o^2 - F_c^2)^2]/\sum[w(F_o^2)^2]]^{1/2}$; $w = 1/[\sigma^2(F_o^2) + (mP)^2 + nP]$ where $P = (F_o^2 + 2F_c^2)/3$. $m = 0.0966$ [**1**(LS)], 0.1027 [**1**(130 K)], and 0.0552 [**1**(HS)]; $n = 3.6684$ [**1**(LS)], 14.6044 [**1**(130 K)], and 0.0000 [**1**(HS)].

X-ray Crystallography. Diffraction data on crystals of **1** were collected at 293 and 130 K as well as at 293 K. After the crystals were warmed to 360 K, **2** was collected at three temperatures [360 (Supporting Information), 293, and 140 K], while **3**−**5** were collected at 293 K with a Nonius Kappa CCD single-crystal diffractometer using Mo Kα (λ = 0.710 73 Å). A multiscan absorption correction was performed but not applied. The absorption correction was found to have no significant effect on the refinement results. The structures were solved by direct methods using *SHELXS-97* and refined by full-matrix least squares on F^2 using *SHELXL-97*.[20] All non-H atoms were refined anisotropically. Relevant crystallographic data and selected bond lengths for **1**−**5** are displayed in Tables 1−7.

Results

Magnetic Properties. The thermal dependence of the $\chi_M T$ product for compound **1** is displayed in Figure 1, with χ_M being the molar magnetic susceptibility and T the temperature. For **1**, $\chi_M T$ is equal to 0.68 cm^3 K mol^{-1} at 300 K, a value that indicates that the majority of the iron(II) centers are in the LS state. Upon cooling, $\chi_M T$ decreases smoothly down to 0.29 cm^3 K mol^{-1} at ca. 150 K, a value that remains practically constant below this temperature. In the warming mode, the magnetic behavior is identical with the cooling mode in the 5−300 K temperature interval. However, for temperatures higher than 300 K, $\chi_M T$ increases rapidly, reaching a value of 3.55 cm^3 K mol^{-1} at 390 K, indicating a complete conversion from the LS state to the HS state. Once this temperature was attained, the magnetic behavior of **1** was again recorded in the cooling mode. In this mode,

(18) Galet, A.; Gaspar, A. B.; Muñoz, M. C.; Real, J. A. *Chem. Commun.* **2003**, 1248.
(19) Galet, A.; Muñoz, M. C.; Real, J. A. *Inorg. Chem.* **2006**, *45*, 4583.
(20) Sheldrick, G. M. *SHELX97: Program for Crystal Structure Determination*; University of Gottingen: Gottingen, Germany, 1997.

Table 2. Crystal Data for **2**[a]

	293 K	140 K
empirical formula	$C_{24}H_{16}N_8Cl_4Cu_2Fe$	
M_r	741.18	
cryst syst	monoclinic	
space group	$P2_1/c$	
a (Å)	17.7190(4)	17.3740(5)
b (Å)	8.9740(2)	8.7380(2)
c (Å)	23.9950(5)	23.5790(6)
β (deg)	125.9400(10)	126.243(2)
V (Å^3)	3089.11(12)	2887.02(13)
Z	4	
D_c (mg cm^{-3})	1.594	1.705
F(000)	1472	
μ(Mo Kα) (mm^{-1})	2.202	2.356
cryst size (mm)	0.03 × 0.04 × 0.04	
no. of total reflns	7020	6548
no. of reflns [$I > 2\sigma(I)$]	3749	4326
R1 [$I > 2\sigma(I)$]	0.0746	0.0647
wR [$I > 2\sigma(I)$]	0.2079	0.1448
S	0.844	1.028

[a] $R1 = \sum||F_o| - |F_c||/\sum|F_o|$; $wR = [\sum[w(F_o^2 - F_c^2)^2]/\sum[w(F_o^2)^2]]^{1/2}$; $w = 1/[\sigma^2(F_o^2) + (mP)^2 + nP]$ where $P = (F_o^2 + 2F_c^2)/3$. $m = 0.1551$ [**5**(293 K)], 0.0620 [**5**(140 K)]; $n = 15.6167$ [**5**(293 K)], 14.1956 [**5**(140 K)].

Table 3. Crystal Data for **3**−**5**[a]

	3(293 K)	**4**(293 K)	**5**(293 K)
empirical formula	$C_{24}H_{16}N_8Cl_4Cu_2Fe$	$C_{24}H_{16}N_8Br_4Cu_2Fe$	$C_{24}H_{16}N_8I_4Cu_2Fe$
M_r	741.18	919.02	1106.98
cryst syst	triclinic	triclinic	triclinic
space group	$P\bar{1}$	$P\bar{1}$	$P\bar{1}$
a (Å)	8.2580(3)	8.2650(5)	8.3870(6)
b (Å)	8.3580(3)	8.4710(6)	8.6050(7)
c (Å)	10.2050(4)	10.2680(8)	10.4070(9)
α (deg)	89.6450(10)	90.866(3)	92.575(4)
β (deg)	87.8330(10)	92.670(3)	92.975(3)
γ (deg)	88.945(2)	90.244(4)	92.992(2)
V (Å^3)	703.72(5)	718.02(9)	748.18(10)
Z	1	1	1
D_c (mg cm^{-3})	1.749	2.125	2.457
F(000)	368	440	512
μ (Mo−K$_\zeta$) (mm^{-1})	2.416	7.561	6.043
cryst size (mm)	0.08 × 0.09 × 0.10	0.06 × 0.07 × 0.09	0.04 × 0.06 × 0.07
no. of total reflns	3188	3135	3349
no. of reflns [$I > 2\sigma(I)$]	2368	1523	2390
R1 [$I > 2\sigma(I)$]	0.0361	0.0792	0.0556
wR [$I > 2\sigma(I)$]	0.0947	0.1653	0.1320
S	0.959	1.003	1.041

[a] $R1 = \sum||F_o| - |F_c||/\sum|F_o|$; $wR = [\sum[w(F_o^2 - F_c^2)^2]/\sum[w(F_o^2)^2]]^{1/2}$; $w = 1/[\sigma^2(F_o^2) + (mP)^2 + nP]$ where $P = (F_o^2 + 2F_c^2)/3$. $m = 0.0608$ (**2**), 0.0953 (**3**), and 0.0740 (**4**); $n = 1.2504$ (**2**), 4.2536 (**3**), and 3.8312 (**4**).

$\chi_M T$ decreases smoothly down to 2.43 cm^3 K mol^{-1} at 230 K. Then, it decreases much more rapidly between 230 and 100 K, where $\chi_M T$ is equal to 0.35 cm^3 K mol^{-1}. The critical temperature for this subsequent, more cooperative spin conversion is 187 K. For lower temperatures, $\chi_M T$ remains practically constant. In the warming mode, the $\chi_M T$ vs T curve is identical with that recorded from 390 K in the cooling mode. This behavior was reproduced four times more, showing the irreversible nature of the first transition.

The magnetic behavior of **2** is displayed in Figure 2. At 360 K, $\chi_M T$ is 3.21 cm^3 K mol^{-1}, indicating that the majority of the iron(II) centers are in the HS state. When cooling, it shows a slight tendency to decrease, attaining a value of 3.15 cm^3 K mol^{-1} at 300 K. From this temperature, $\chi_M T$ decreases moderately down to 240 K (2.88 cm^3 K mol^{-1}) and then much more rapidly to attain a value of 0.16 cm^3 K mol^{-1} at 100 K. The shape of the $\chi_M T$ vs T curve denotes the occurrence of a not well-resolved, almost complete, two-step spin transition with very close critical temperatures $T_{c1} = 169$ K and $T_{c2} = 210$ K. The warming mode describes exactly the same curve, indicating that the possible hysteresis loop should be smaller than 1 K.

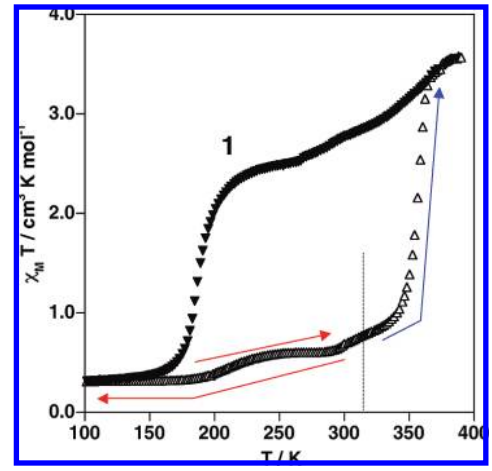

Figure 1. Magnetic behavior of **1**. Red arrows indicate the experimental data in the cooling-warming cycle before surpassing 330 K (vertical dotted line). Blue arrow indicates the irreversible change of $\chi_M T$. Filled triangles represent the reversible new magnetic behavior after heating the **1** up to 360 K.

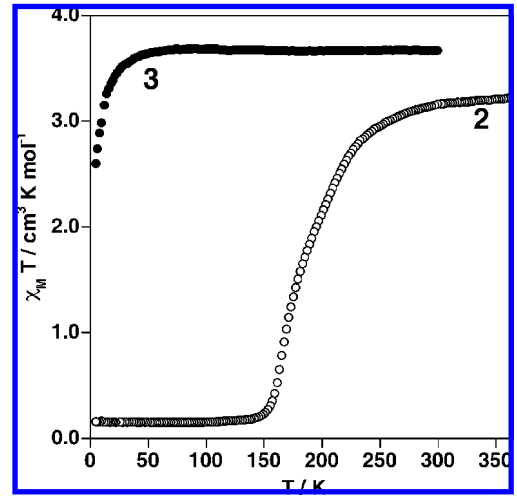

Figure 2. Magnetic behavior of **2** (open circles) and **3** (filled circles).

$\chi_M T$vs T plots are similar for compounds **3**−**5**. Figure 2 displays the magnetic behavior of compound **3**, while $\chi_M T$ vs T plots for **4** and **5** are given in the Supporting Information. At 300 K, $\chi_M T$ is around 3.70 cm^3 K mol^{-1} and remains almost constant upon cooling for **3**. Below 50 K, $\chi_M T$ decreases, showing the characteristic zero-field splitting of the $S = 2$ ground state of the Fe^{II} ion. Consequently, these compounds are HS in the whole range of temperatures investigated.

Crystal Structure. Crystal Structure of 1. The crystal structure of **1** has been studied at 293 and 130 K and at 293 K after warming the crystal to 360 K (293 K*). This compound displays the monoclinic $P2_1/c$ spatial group at all

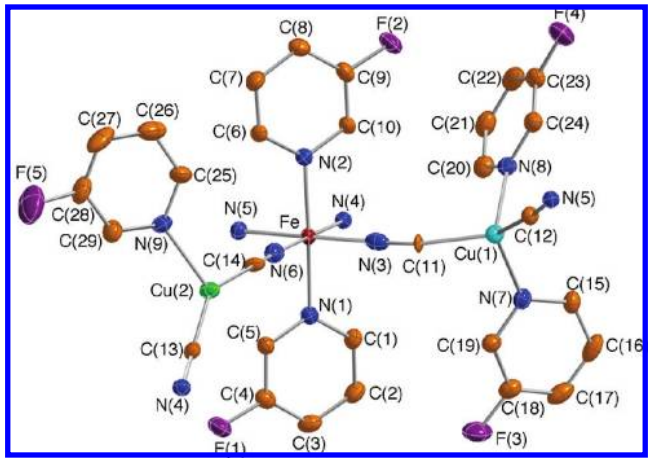

Figure 3. ORTEP representation of the asymmetric unit of **1** (293 K) and its corresponding atom numbering. Thermal ellipsoids are presented at 30% of probability.

Table 4. Selected Bond Lengths [Å] and Angles [deg] for **1**[a]

	293 K	130 K	293 K*
Fe−N(1)	2.030(4)	2.009(8)	2.198(7)
Fe−N(2)	2.031(4)	2.023(8)	2.193(7)
Fe−N(3)	1.943(5)	1.943(12)	2.081(8)
Fe−N(4)	1.984(4)	1.981(8)	2.112(7)
Fe−N(5)	1.969(4)	1.968(8)	2.076(7)
Fe−N(6)	1.924(6)	1.934(11)	2.096(8)
Cu(1)−N(7)	2.123(5)	2.118(7)	2.141(7)
Cu(1)−N(8)	2.215(4)	2.178(8)	2.234(8)
Cu(1)−C(11)	1.964(4)	1.986(8)	1.949(9)
Cu(1)−C(12)	1.893(5)	1.886(10)	1.882(8)
Cu(2)−N(9)	2.102(4)	2.085(8)	2.083(7)
Cu(2)−C(13)	1.875(5)	1.880(11)	1.889(9)
Cu(2)−C(14)	1.878(4)	1.856(9)	1.872(9)
N(1)−Fe−N(2)	177.6(2)	177.4(3)	178.1(3)
N(1)−Fe−N(3)	91.5(2)	91.7(3)	91.0(3)
N(1)−Fe−N(4)	89.3(2)	89.6(3)	89.6(3)
N(1)−Fe−N(5)	88.7(2)	88.7(3)	88.5(3)
N(1)−Fe−N(6)	89.8(2)	89.7(3)	89.9(3)
N(2)−Fe−N(3)	90.9(2)	90.9(3)	90.9(3)
N(2)−Fe−N(4)	90.3(2)	90.3(3)	90.9(3)
N(2)−Fe−N(5)	88.9(2)	88.8(3)	89.7(3)
N(2)−Fe−N(6)	90.5(2)	90.4(3)	89.6(3)
N(3)−Fe−N(4)	91.0(2)	91.0(3)	90.4(2)
N(3)−Fe−N(5)	179.5(2)	179.5(3)	178.6(3)
N(3)−Fe−N(6)	88.9(2)	88.7(4)	89.3(3)
N(4)−Fe−N(5)	88.6(2)	89.3(3)	90.8(2)
N(4)−Fe−N(6)	179.1(2)	179.3(4)	179.4(3)
N(5)−Fe−N(6)	91.6(2)	91.0(3)	89.4(3)
N(7)−Cu(1)−N(8)	100.8(2)	102.1(3)	102.0(3)
C(11)−Cu(1)−N(7)	96.5(2)	96.5(3)	98.6(3)
C(12)−Cu(1)−N(7)	120.5(2)	121.8(3)	117.6(3)
C(11)−Cu(1)−N(8)	95.7(2)	95.4(3)	95.1(3)
C(12)−Cu(1)−N(8)	106.8(2)	108.1(4)	106.0(3)
C(12)−Cu(1)−C(11)	130.7(2)	127.7(4)	131.9(3)
C(13)−Cu(2)−N(9)	111.9(2)	113.3(3)	106.9(3)
C(14)−Cu(2)−N(9)	103.8(2)	104.0(3)	109.9(3)
C(13)−Cu(2)−C(14)	144.3(2)	142.7(4)	143.0(4)

[a] 293 K* stands for the crystal structure of **1** at 293 K after irreversible spin transition above 330 K.

temperatures studied. The structure is constituted of three geometrically distinct building blocks: a slightly distorted $[FeN_6]$ octahedral site, a pseudotetrahedral $[Cu(1)C_2N_2]$ site, and a pseudotrigonal $[Cu(2)C_2N]$ site. Figure 3 displays the asymmetric unit of **1**, and Table 4 contains a selection of the corresponding bond distances and angles. The equatorial positions of the Fe atom are occupied by the N atoms of four cyanide groups belonging to two crystallographically distinct Cu(1) and Cu(2) sites: Fe−N(3) = 1.943(5) Å, Fe−N(4) = 1.984(4) Å, Fe−N(5) = 1.969(4) Å, and Fe−N(6) = 1.924(6) Å bond distances at 293 K. The axial positions are occupied by two N atoms of two crystallographically different 3-Fpy ligands whose Fe−N bond lengths are Fe−N(1) = 2.030(4) Å and Fe−N(2) = 2.031(4) Å at 293 K. The average bond length $Fe-N_{av}$ = 1.980(5) Å as well as the angles around the $[FeN_6]$ site (close to 90° or 180°) indicate that the Fe^{II} ion is essentially in the LS state, in agreement with the magnetic properties.

The pseudotetrahedral $[Cu(1)C_2N_2]$ and pseudotrigonal $[Cu(2)C_2N]$ sites are defined by the in situ generated $[Cu(1)(3\text{-Fpy})_2(CN)_2]^-$ and $[Cu(2)(3\text{-Fpy})(CN)_2]^-$ bridging moieties. The two Cu(1)−N distances are considerably longer than the Cu(1)−C ones: Cu(1)−N(7) = 2.123(5) Å and Cu(1)−N(8) = 2.215(4) Å vs Cu(1)−C(11) = 1.964(4) Å and Cu(1)−C(12) = 1.893(5) Å. The angles strongly deviate from what is expected for a regular tetrahedron (109.5°) [N(7)−Cu(1)−N(8) = 100.8(2)°, C(11)−Cu(1)−N(7) = 96.5(2)°, C(12)−Cu(1)−N(7) = 120.5(2), C(11)−Cu(1)−N(8) = 95.7(2)°, C(12)−Cu(1)−N(8) = 106.8(2)°, C(12)−Cu(1)−C(11) = 130.7(2)°]. The four atoms of the pseudotrigonal site lie practically in the same plane with the Cu(2)−N(9) bond distance, 2.102(4) Å, much longer than Cu(2)−C(13) = 1.875(5) Å and Cu(2)−C(14) = 1.878(4) Å. The corresponding bond angles strongly deviate from 120° [C(13)−Cu(2)−N(9) = 111.9(2)°, C(14)−Cu(2)−N(9) = 103.8(2)°, and C(13)−Cu(2)−C(14) = 144.3(2)°].

At 130 K, Fe−N(1) decreases significantly, by ca. 0.021 Å, whereas the other bond distances and angles of the $[FeN_6]$ site remain practically unaltered. Some significant modifications are also observed in the $[Cu(1)C_2N_2]$ and $[Cu(2)C_2N]$ sites at this temperature: Cu(1)−C(11) increases by 0.022 Å; Cu(1)−N(8), Cu(2)−N(9), and Cu(2)−C(14) decrease by 0.037, 0.017, and 0.022 Å, respectively. Simultaneously, the angles N(7)−Cu(1)−N(8), N(7)−Cu(1)−C(12), N(8)−Cu(1)−C(12), and C(13)−Cu(2)−N(9) increase by ca. 1.3°, while C(12)−Cu(1)−C(11) and C(13)−Cu(2)−C(14) decrease by ca. 3.0° and 1.6°, respectively.

The three building blocks are interconnected, defining edge-sharing $[Fe_4]$ squares (9.356 × 9.298 Å). The edges of the squares strongly deviate from 180° because the angles defined by the connectors are C(12)−Cu(1)−C(11) = 130.7(2)° and C(13)−Cu(2)−C(14) = 144.3(2)° (Figure 4a). Furthermore, the Cu(1) and Cu(2) atoms are respectively 1.650(2) and 1.623(2) Å out of the plane containing the four Fe atoms but in opposite directions. Consequently, the $[FeN_6]$ octahedra are markedly tilted, generating strongly corrugated 2D layers, which spread on the *yz* plane and stack along the *z* axis (Figure 4b). Two consecutive layers are organized in such a way that the Fe atoms of one layer project at a distance of 8.467(2) Å over the baricenter of the $[Fe_4]$ squares of contiguous layers. The space between two consecutive layers is filled with the 3-Fpy ligands. Furthermore, the 3-Fpy ligands of the Cu(1), Cu(2), and Fe sites of consecutive layers are interdigitated along the [001] direction defining 1D chains. Within these chains, strong π interactions, which

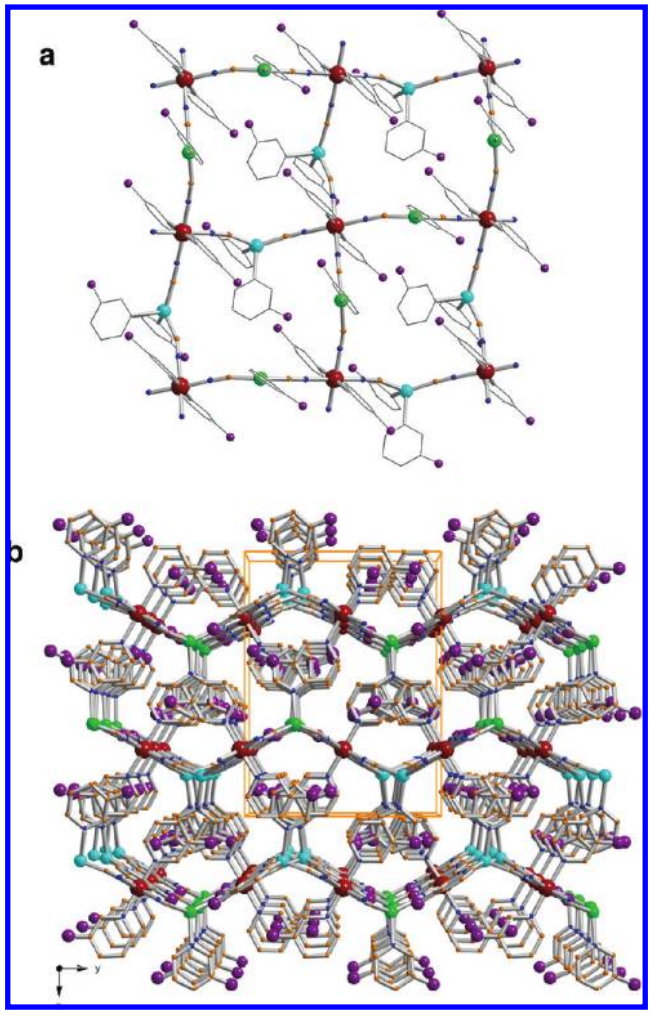

Figure 4. (a) View of a grid showing the distorted square windows generated by two pseudotetrahedral $[Cu(1)(3\text{-}Fpy)_2(CN)_2]^-$ and two pseudotrigonal $[Cu(2)(3\text{-}Fpy)(CN)_2]^-$ bridging moieties of **1**. (b) View along the [001] direction of three consecutive corrugated layers of **1** illustrating the generation of strong interactions between 3-Fpy ligands along the *z* axis.

depend on the Fe^{II} spin state, are observed. In general, they are shorter in the LS state (Table 5).

Trying to gain some insight into the irreversible magnetic behavior described above, the same crystal was heated from 130 K up to 360 K; then it was cooled, and a new data set was collected at 293 K. After this thermal treatment, the average axial and equatorial distances at 293 K* [$Fe-N_{axial}$ = 2.195(7) Å and $Fe-N_{equatorial}$ = 2.091(8) Å] were respectively 0.179 and 0.135 Å larger than the corresponding values at 130 K and 0.165 and 0.136 Å larger than those at 293 K before thermal treatment. The average Fe−N bond length distance in the $[FeN_6]$ octahedron is 0.146 Å larger at 293 K after thermal treatment. This value is consistent with ca. 75% of the Fe^{II} atoms in the HS state, a fact that agrees with the magnetic data. The changes around the $[Cu(1)C_2N_2]$ and $[Cu(2)C_2N]$ sites are, with respect to the 130 K structure, more marked after thermal treatment. For example, the Cu(1)−N(7) and Cu(1)−N(8) bond lengths are 0.023 and 0.056 Å larger, respectively, while the Cu(1)−C(11) bond length is 0.037 Å smaller. Furthermore, remarkable bond angle variations are observed for C(12)−Cu(1)−N(7), C(13)−Cu(2)−N(9), C(12)−Cu(1)−C(11), and C(14)−Cu(2)−N(9), which change by −4.2°, −6.4°, 4.2°, and 5.9°, respectively.

Table 5. Selected Intermolecular Contacts [Å] for **1**[a]

	293 K	293 K*
C(1)···C(16)^{i}	3.579(9)	3.608(13)
C(2)···C(16)^{i}	3.647(9)	3.743(13)
C(3)···C(16)^{i}	3.650(9)	3.738(13)
C(2)···C(15)^{i}	3.439(8)	3.514(12)
C(2)···C(19)^{ii}	3.589(8)	3.575(12)
C(3)···C(15)^{i}	3.515(8)	3.583(11)
C(3)···C(18)^{ii}	3.546(9)	3.613(12)
C(3)···C(19)^{ii}	3.300(8)	3.333(10)
C(4)···C(17)^{ii}	3.526(9)	3.589(12)
C(4)···C(18)^{ii}	3.504(8)	3.559(12)
C(5)···C(16)^{i}	3.506(8)	3.502(12)
C(5)···C(17)^{ii}	3.597(8)	3.645(12)
C(5)···C(18)^{ii}	3.660(8)	3.673(11)
C(7)···C(25)^{iii}	3.696(9)	3.697(12)
C(8)···C(25)^{iii}	3.608(9)	3.649(11)
C(8)···C(29)^{iv}	3.617(9)	3.631(11)
C(9)···C(25)^{iv}	3.671(9)	3.626(12)
C(9)···C(26)^{iv}	3.469(10)	3.553(13)
C(9)···C(27)^{iv}	3.495(10)	3.645(13)
C(10)···C(26)^{iii}	3.633(9)	3.501(11)
C(10)···C(27)^{ii}	3.521(10)	3.542(12)
C(10)···C(27)^{iv}	3.515(10)	3.571(12)

[a] 293 K* stands for the crystal structure of **1** at 293 K after irreversible spin transition above 330 K. Symmetry codes: i, $-x$, $y - 1/2$, $-z + 1/2$; ii, $-x$, $-y$, $-z$; iii, $-x + 1$, $y + 1/2$, $-z + 1/2$; iv, $-x + 1$, $-y$, $-z + 1$.

Table 6. Selected Bond Lengths [Å] and Angles [deg] for **2**

	293 K	140 K
Fe(1)−N(1)	2.211(7)	2.004(5)
Fe(1)−N(2)	2.095(6)	1.943(5)
Fe(1)−N(3)	2.101(7)	1.938(5)
Fe(2)−N(4)	2.211(7)	2.010(5)
Fe(2)−N(5)	2.126(6)	1.948(5)
Fe(2)−N(6)	2.134(7)	1.953(5)
Cu(1)−N(7)	2.120(8)	2.121(5)
Cu(1)−C(6)	1.877(7)	1.899(6)
Cu(1)−C(13)	1.898(8)	1.912(6)
Cu(2)−N(8)	2.113(7)	2.124(5)
Cu(2)−C(7)	1.872(8)	1.892(6)
Cu(2)−C(14)	1.892(8)	1.889(6)
N(1)−Fe(1)−N(2)	90.3(3)	90.2(2)
N(1)−Fe(1)−N(3)	90.5(3)	90.7(2)
N(2)−Fe(1)−N(3)	89.7(3)	90.5(2)
N(4)−Fe(2)−N(5)	90.1(3)	90.2(2)
N(4)−Fe(2)−N(6)	89.6(3)	89.2(2)
N(5)−Fe(2)−N(6)	91.5(2)	91.6(2)
N(7)−Cu(1)−C(6)	110.1(3)	108.2(2)
N(7)−Cu(1)−C(13)	103.9(3)	102.6(2)
C(6)−Cu(1)−C(13)	145.6(3)	148.5(2)
N(8)−Cu(2)−C(7)	107.5(3)	105.2(2)
N(8)−Cu(2)−C(14)	108.3(3)	106.8(2)
C(7)−Cu(2)−C(14)	144.1(3)	147.9(2)

Crystal Structure of 2. The crystal structure of **2** has been investigated at 140, 293, and 360 K (see the Supporting Information). It is constituted of two crystallographically different, slightly distorted $[FeN_6]$ octahedral sites and two pseudotrigonal $[CuC_2N]$ sites (Table 6). The Fe^{II} sites are placed in an inversion center with the equatorial positions occupied by the in situ formed trigonal anionic bridges $[Cu(3\text{-}Clpy)(CN)_2]^-$, whereas the axial positions are occupied by the 3-Clpy ligand. At 140 K, the $Fe-N_{equatorial}$ bond lengths are Fe(1)−N(2) = 1.943(5) Å, Fe(1)−N(3) = 1.938(5) Å, Fe(2)−N(5) = 1.948(5) Å, and Fe(2)−N(6) = 1.953(5) Å, while the $Fe-N_{axial}$ bond lengths are Fe(1)−N(1) = 2.004(5)

Table 7. Selected Bond Lengths [Å] and Angles [deg] for **3**−**5**

	3(293 K)	**4**(293 K)	**5**(293 K)
Fe−N(1)	2.268(3)	2.256(11)	2.270(7)
Fe−N(2)	2.139(3)	2.156(11)	2.168(7)
Fe−N(3)	2.146(3)	2.164(11)	2.172(7)
Cu−N(4)	2.052(3)	2.053(9)	2.072(7)
Cu−C(6)	1.911(4)	1.907(12)	1.925(9)
Cu−C(7)	1.910(4)	1.926(14)	1.929(10)
N(1)−Fe−N(2)	89.86(13)	90.0(4)	89.5(3)
N(1)−Fe−N(3)	88.97(13)	89.1(4)	89.7(3)
N(2)−Fe−N(3)	89.01(13)	89.8(4)	90.8(3)
C(6)−Cu−N(4)	118.62(14)	120.2(5)	121.7(3)
C(7)−Cu−N(4)	114.55(14)	114.5(5)	110.2(3)
C(7)−Cu−C(6)	125.8(2)	123.9(5)	126.2(4)

Å and Fe(2)−N(4) = 2.010(5) Å (Figure 5a,b). The angles around the [FeN_6] sites are close to those expected for a regular octahedron, with the maximum deviation being less than 2°. The Cu^I sites are almost in the plane defined by the donor atoms: Cu(1) and Cu(2) are 0.080(5) and 0.027(5) Å out of the plane defined by C(13)−C(6)−N(7) and C(14)−C(7)−N(8), respectively. The Cu−C bond distances are significantly shorter than the Cu−N ones: Cu(1)−C(13) = 1.912(6) Å, Cu(1)−C(6) = 1.899(6) Å, Cu(2)−C(14) = 1.889(6) Å, Cu(2)−C(7) = 1.892(6) Å, Cu(1)−N(7) = 2.121(5) Å, and Cu(2)−N(8) = 2.124(5) Å. The angles of the trigonal plane differ considerably from 120°: C(13)−Cu(1)−C(6) = 148.5(2)°, C(14)−Cu(2)−C(7) = 147.9(2)°, C(6)−Cu(1)−N(7) = 108.2(2)°, C(13)−Cu(1)−N(7) = 102.6(2)°, C(7)−Cu(2)−N(8) = 105.2(2)°, and C(14)−Cu-(2)−N(8) = 106.8(2)°. Each $[Cu(3\text{-}Clpy)(CN)_2]^-$ species bridges two Fe atoms in such a way that one Fe site, i.e., Fe(1), is surrounded by four Fe(2) sites and vice versa, thereby forming a relatively uncommon 3D network with the topology of $CdSO_4$ (Figure 6a). A view of the network in the [010] direction shows that the framework is compartmentalized in apparently squarelike motives, whose Fe···Fe edges make 9.662 × 9.724 Å. In fact, these "squarelike" motives correspond to a projection of infinite square helices made up of [Fe−NC−Cu−CN−Fe] moieties (Figure 6b). The four quadrants defined by the $[Cu(3\text{-}Clpy)(CN)_2]^-$ bridges at each Fe site define four of such helices that have opposite helicity. These helicoidal channels are filled with the 3-Clpy groups coordinated to the Cu sites, which point toward the center of the helicoidal channels (Figure 6c).

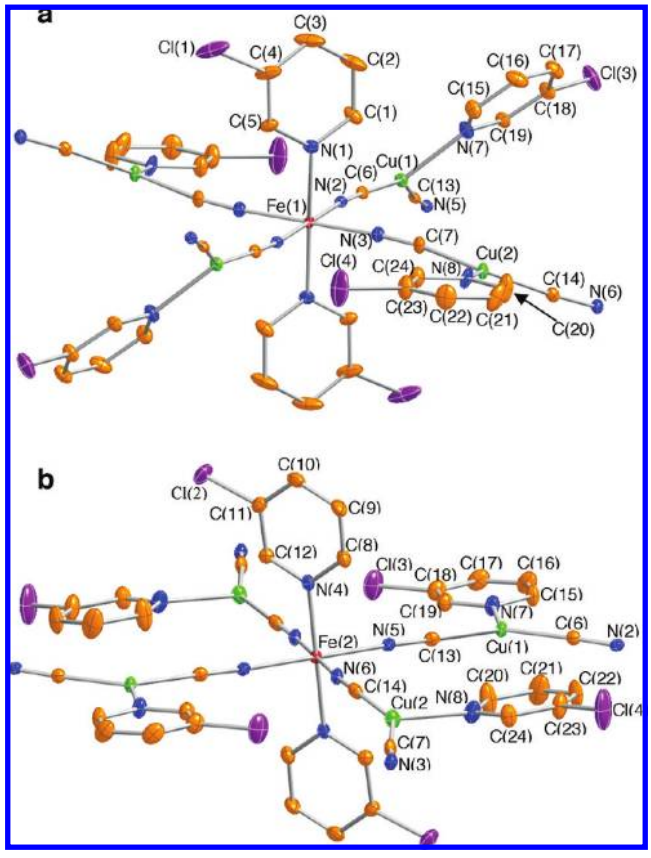

Figure 5. ORTEP representation of the two asymmetric units of **2** (140 K) and their corresponding atom numbering. Thermal ellipsoids are presented at 30% of probability.

At 293 K, **2** displays the characteristic structural changes associated with a LS-to-HS Fe^{II} spin conversion. The axial Fe−N bond distances show significantly larger variations than the equatorial ones: $\Delta[Fe(1)-N(1)]_{ax}$ = 0.207 Å, $\Delta[Fe(2)-N(4)]_{ax}$ = 0.201 Å, $\Delta[Fe(1)-N(2)]_{eq}$ = 0.152 Å, $\Delta[Fe(1)-N(3)]_{eq}$ = 0.163 Å, $\Delta[Fe(2)-N(5)]_{eq}$ = 0.178 Å, and $\Delta[Fe(2)-N(6)]_{eq}$ = 0.181 Å. The average increase of the [FeN_6] bond distances, 0.174 and 0.187 Å for Fe(1) and Fe(2), respectively, is close to that typically observed (ca. 0.2 Å) and suggests the occurrence of about 10% of Fe^{II} sites in the LS state at 293 K. There are no significant variations of the [FeN_6] coordination core angles upon spin-state change except for Fe(1)−N(3)−C(7) and Fe(2)−N(6)−C(14), which are respectively 4.3° and 8.0° smaller at 293 K. The coordination surroundings of the Cu sites are little affected as a consequence of the spin-state change. The most remarkable variations correspond to the C(13)−Cu(1)−C(6) and C(14)−Cu(2)−C(7) angles, which decrease by 2.9° and 3.8°, respectively.

At 360 K, the change of the average Fe−N bond distances is insignificant with respect to 293 K. In spite of this, the individual Fe−N distances display significant changes of opposite sign, which almost cancel each other out. For instance, Fe(1)−N(1) decreases 0.027 Å, while Fe(1)−N(3) increases 0.034 Å. Similarly, Cu(1)−N(7) and Cu(1)−C(13) increase 0.025 and 0.021 Å, respectively, while Cu(2)−C(7) decreases 0.023 Å.

The volume of the unit cell increases 201.98 or 50.49 $Å^3$ per Fe atom when warming from 140 to 293 K. An additional variation of 34 Å (8.5 $Å^3$ per Fe) is observed when moving from 293 to 360 K.

Crystal Structures of 3−5. Compounds **3**−**5** are isostructural and crystallize in the $P\bar{1}$ triclinic space group. Figure 7 depicts a representative fragment of **3**−**5** structures together with the corresponding atom numbering. Table 7 displays representative bond lengths and angles of **3**−**5**. As in the previous structure, the building blocks are the pseudooctahedral Fe^{II} cations and the $[Cu(3\text{-}Xpy)(CN)_2]^-$ bridging anions; however, in the present case, they originate a different coordination polymer. The Fe^{II} atom located at an inversion center defines an elongated octahedron. The axial coordination positions are occupied by two crystallographically

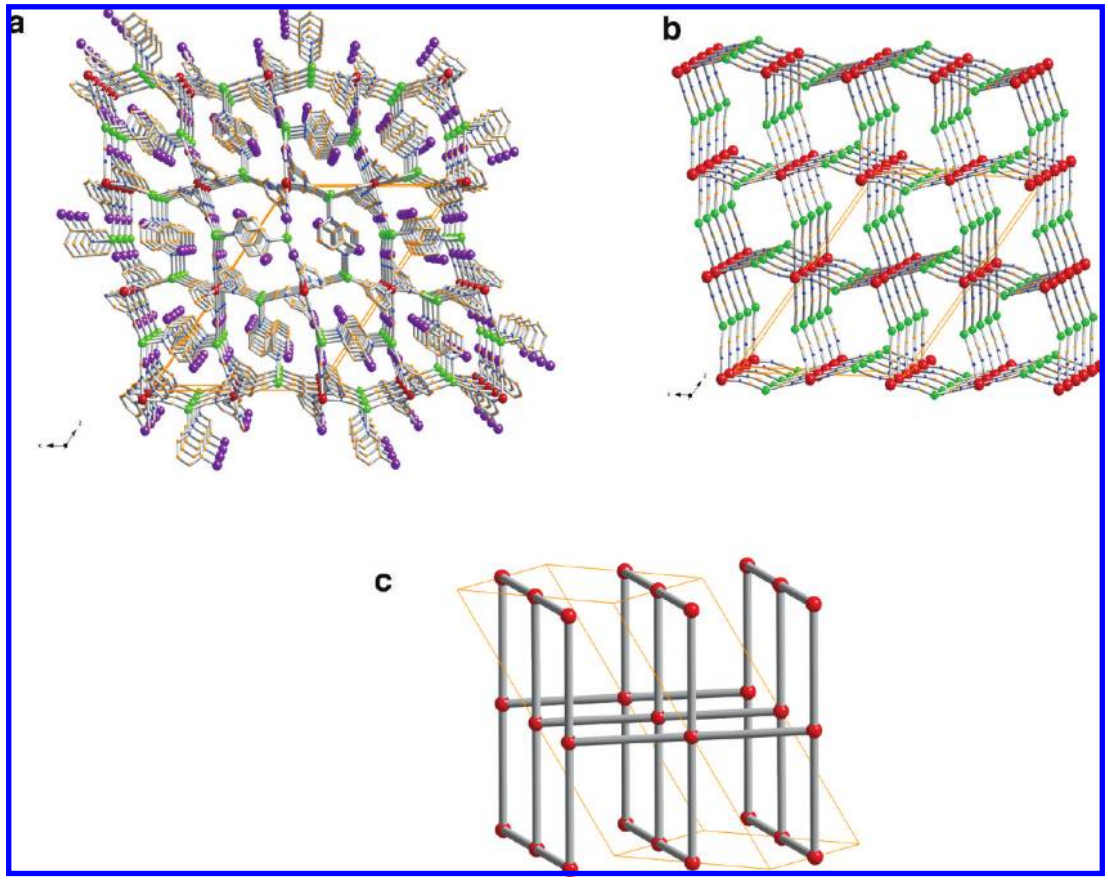

Figure 6. Fragment of the 3D network **2** with (a) and without (b) the ligand 3-Clpy. Schematic view of the structural motive representing an expanded version of the $CdSO_4$-type structure (c).

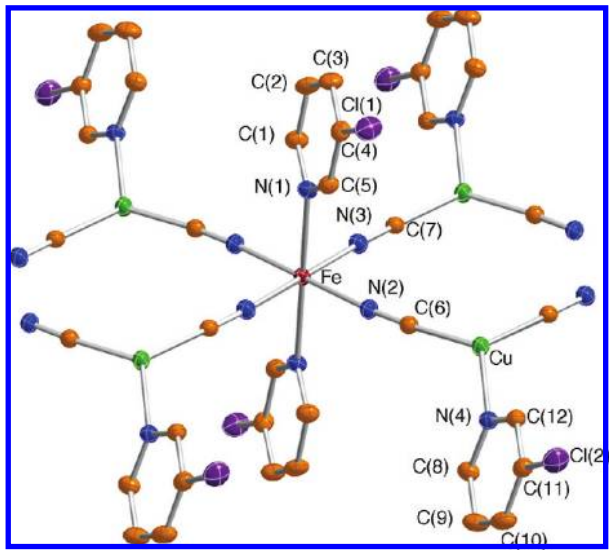

Figure 7. ORTEP representation of the asymmetric unit of **3** (293 K) and its corresponding atom numbering. Thermal ellipsoids are presented at 30% of probability.

equivalent 3-Xpy ligands, and the four equatorial positions are occupied by the $[Cu(3\text{-}Xpy)(CN)_2]^-$ (X = Cl, Br, and I) anions. The axial Fe−N(1) bond distances are 2.268(3) (**3**), 2.256(11) (**4**), and 2.270(7) (**5**) Å. The equatorial bond lengths are Fe−N(2) = 2.139(3), 2.156(11), and 2.168(7) Å and Fe−N(3) = 2.146(3), 2.164(11), and 2.172(7) Å for **3**−**5**, respectively. The trigonal-planar coordination geometry defined by the Cu^{II} ion is more regular than that in **2**. Indeed, the Cu−C distances [Cu−C(6) = 1.911(4) (**3**), 1.907(12) (**4**), and 1.925(9) (**5**) Å and Cu−C(7) = 1.910(4) (**3**), 1.926(14) (**4**), and 1.929(10) (**5**) Å] are slightly longer, while the Cu−N bond distances are markedly shorter [Cu−N(4) = 2.052(3) (**3**), 2.053(9) (**4**), and 2.072(7) (**5**) Å]. The bond angles around the Cu^I atom are, in general, much closer to 120° than those in **2** [C(7)−Cu−C(6) = 125.8(2)° (**3**), 123.9(5)° (**4**), and 126.2(4)° (**5**); N(4)−Cu−C(6) = 118.62(14)° (**3**), 120.2(5)° (**4**), and 121.7(3)° (**5**), and C(7)−Cu−N(4) = 114.55(14)° (**3**), 114.5(5)° (**4**), and 110.2(3)° (**5**)]. These structural characteristics determine a different propagation for the coordination building blocks in the polymer, defining infinite chains running along the [100] direction. These chains superpose perfectly in the [010] direction, defining layers in which adjacent chains interdigitate the 3-Xpy groups coordinated to the iron and copper centers. The layers stack along the [001] direction. No significant intermolecular interactions have been observed (Figure 8).

Discussion

This work was undertaken with the aim of investigating new bimetallic iron(II)−metal(I) cyanide-based SCO metal−organic frameworks containing 3-Xpy ligands (X = F, Cl, Br, and I). As mentioned in the Introduction section, we have already reported the series with M^I = Ag and Au, where the synthesis, crystal structures, and magnetic properties of the compounds $\{Fe(3\text{-}Xpy)_2[M(CN)_2]_2\}$ were described. Here we complete this study by investigating the corresponding

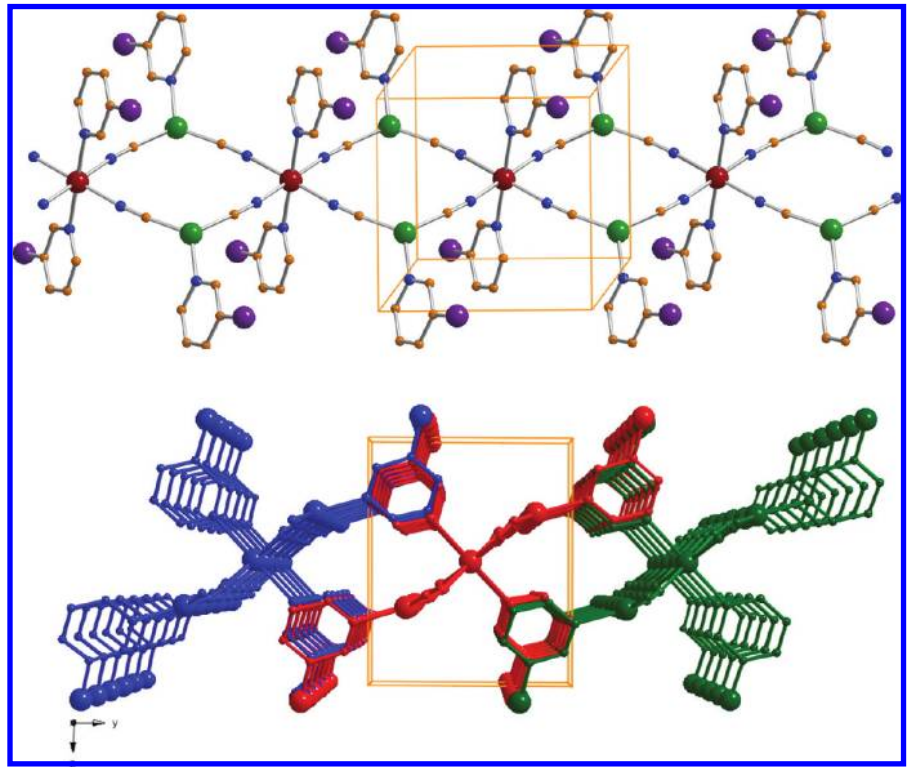

Figure 8. Representation of a fragment of a chain of **3** running along the *x* axis (top) and view of three adjacent chains showing interdigitation between 3-Xpy groups (bottom).

copper(I) derivatives. Several differences deserve to be pointed out with respect to the silver(I) and gold(I) derivatives. An important singular feature is the in situ coordination of one or even two 3-Xpy ligands to the linear $[Cu(CN)_2]^-$ anion, giving a new folded bridging ligand formulated as $[Cu(3\text{-}Xpy)_z(CN)_2]^-$ ($z = 1$ and 2). This fact occurs for the whole series, X = F, Cl, Br, and I, working under conditions similar to those used for the synthesis of $\{Fe(3\text{-}Xpy)_2[M(CN)_2]_2\}$ (M^I = Ag and Au). Expansion of the copper(I) coordination number from two to three ($z = 1$) was previously observed in the 1D SCO polymer $\{Fe(3\text{-}CNpy)_2[Cu(3\text{-}CNpy)(CN)_2]_2\}$.[19] Such a behavior is uncommon for the silver series and unprecedented for gold derivatives. In fact, it has only been observed in two silver derivatives when an excess of 3-Brpy or 3-Ipy is present in the diffusion vessel.[16] A different way to expand the coordination number of the M^I ion has been previously described when bismonodentate ligands are used. This is the case of the complex $\{Fe(pyrimidine)_2[M(CN)_2]_2\}$ in which the pyrimidine ligands occupy the axial positions of the Fe^{II} ions. When $M = Cu^I$, the pyrimidine ligand bridges the Fe^{II} and Cu^I atoms of adjacent $\{Fe[Cu(CN)_2]\}_n$ chains, forming a 2D polymer with the network topology of $CdCl_2$.[18] In the case of $M = Ag^I$, two architectural 3D isomers are formed. In one isomer, each Fe^{II} and Ag^I atom of adjacent $\{Fe[Ag(CN)_2]_2\}_n$ layers shares one pyrimidine ligand, while in the other isomer, the more corrugated nature of the layers enables coordination of two pyrimidine ligands to one Ag atom of adjacent layers.[14] Expansion of the coordination sphere of Ag^I in $[Ag(CN)_2]^-$ has been described in complexes of the type $\{Fe(L\text{-}L)_2[Ag(CN)_2]_2\}$, where L-L is 4,4′-bipyridine or bis(ethylenepyridine); the larger size of the ligands and their coordination topology enable them to bridge Fe^{II} and Ag^I atoms of alternate layers, giving doubly interpenetrated 3D networks.[10]

Another remarkable feature of the title compounds is the lack of short Cu···Cu contacts smaller than the sum of the van der Waals radius (2.8 Å). The observation of short $M^I \cdots M^I$ contacts in group 11 is usually associated with the occurrence of metallophilic interactions.[21] This is particularly meaningful for compounds involving Ag^I and Au^I atoms, where relativistic effects are expected to be more important than those in Cu^I compounds. In fact, strong metallophilic interactions have been observed in most of the iron(II)−silver(I) and iron(II)−gold(I) coordination polymers, and it has been shown that they play an important role in the cohesive forces of the solid; for example, as mentioned above, they are responsible for the formation of double layers in the $\{Fe(3\text{-}Xpy)_2[M(CN)_2]_2\}$ (M = Ag and Au) series. The nature of intermolecular $Cu^I \cdots Cu^I$ cuprophilic interactions has recently been discussed from a theoretical and structural database analysis.[22] From a theoretical viewpoint, it is difficult to ascertain whether short $Cu^I \cdots Cu^I$ distances correspond to attractive intermetallic interactions because they are expected to be very weak. However, significantly short $Cu^I \cdots Cu^I$ contacts were found to be in the 2.52−2.60 Å range for $\{Fe(3\text{-}CNpy)_2[Cu(3\text{-}CNpy)(CN)_2]_2\}$[19] and $\{Fe(pyrimidine)_2[Cu(CN)_2]_2\}$.[18] These contacts seem to act as additional cohesive forces, organizing the chains of the former and the layers of the latter in 2D and 3D supramolecular arrays, respectively. Like in the 3-CNpy derivative, compounds **3**−**5**

(21) Jansen, M. *Angew. Chem., Int. Ed. Engl.* **1987**, *26*, 1098.
(22) Carvajal, M. A.; Álvarez, S.; Novoa, J. J. *Chem.—Eur. J.* **2004**, *10*, 2117.

also crystallize in the $P\bar{1}$ triclinic space group and are constituted of chains that are similarly organized in the crystal; despite this, the Cu···Cu distances are 4.9972(7), 5.119(2), and 5.371(2) Å for **3**−**5**, respectively.

In contrast to the structural uniformity displayed by the Ag and Au series, the Cu series denotes a certain structural diversity, which deserves to be noted. As mentioned above **3**−**5** are constituted of 1D coordination polymers, while **1** and **2** are respectively 2D and 3D frameworks. Compound **1** is made up of 2D grids constituted by edge-sharing [Fe_4] squares whose edges are defined by distorted trigonal [Cu(3-Fpy)$(CN)_2]^-$and tetrahedral [Cu(3-Fpy)$_2(CN)_2]^-$ anions. Compound **2** represents the first example of a 3D iron(II)−copper(I) cyanide-based coordination polymer. The resulting four-connected network corresponds to an expanded version of the relatively uncommon prototypical $CdSO_4$ net decorated by the 3-Clpy ligands (Figure 1a).[23] This network topology has been previously observed in the SCO compounds {Fe(pmd)(H_2O)[M$(CN)_2]_2$}·H_2O (M = Ag and Au).[12] The much larger intraframework spaces in the latter compounds enabled triple interpenetration of identical frameworks, which interact with each other via metallophilic interactions and strong hydrogen bonds. In contrast to this, the 3-Clpy groups of the [Cu(3-Clpy)$(CN)_2]^-$ bridges fill the void space of the network, preventing interpenetration of identical networks.

Compounds **2** and **3** are architectural isomers because they have exactly the same chemical formula but radically different polymeric structures. Architectural isomers in iron(II)−metal(I) heterobimetallic cyanide-based polymers have been described for the SCO compounds {Fe(3-CNpy)$_2$[Au$(CN)_2]_2$}·$n$$H_2O$ and {Fe(pmd)$_2$[Ag$(CN)_2]_2$} (vide supra). The 3-CNpy system presents three isomers: one consists of triply interpenetrated four-connected 3D networks with the topology of NbO, while the other two polymorphs correspond to two distinct stacks of 2D frameworks, one displaying the typical double layers sustained by strong aurophilic interactions and the other not displaying such interactions. The two former isomers show distinct SCO properties, while the latter is fully HS. Of the two isomers described for {Fe(pmd)$_2$[Ag$(CN)_2]_2$}, only that with a less distorted structure (with the Ag atom in pseudotrigonal geometry) undergoes a cooperative spin transition, while the other, displaying a Ag atom in a pseudotetrahedral coordination environment, remains HS in the whole range of temperature. In a similar way, the isomer compound **2** undergoes a spin conversion, while the isomer **3** is HS. Taking into account that the ligand field strength 10 Dq is proportional to $1/R$,[6] where R represents the average Fe−N distance of the [FeN_6] core, a decrease of 10 Dq of around 9% is estimated for the Fe site of isomer **3** when compared to the Fe site of isomer **2**. This decrease of the metal-to-ligand bond distances can account for the different magnetic behavior observed for both architectural isomers.

As far as the SCO properties are concerned, the magnetic behavior of **1** is interesting. For temperatures smaller than 310 K, the original compound is mostly in the LS state. In fact, at 300 K there is approximately 19% of Fe atoms in the HS state; then this value decreases down to 8% at 130 K (the percentages have been estimated considering $\chi_M T$ = 3.55 cm^3 K mol^{-1} for 100% HS). Consequently, ca. 11% of the Fe atoms reversibly convert into the LS state upon cooling to 130 K. According to these data, the average Fe−N bond distances should decrease by ca. 0.11 × 0.2 Å = 0.022 Å (0.2 Å is the typical average Fe−N bond-length variation), a value directly confirmed from single-crystal X-ray experiments. However, surprisingly, this Fe−N bond-length variation is assumed only by one Fe−N bond distance, Fe−N(1), which changes by ca. 0.021 Å. Furthermore, the Cu^I sites apparently seem to be strongly coupled with this residual change of the spin state. The Cu(1)−C(11) bond length increases by 0.022 Å, and simultaneously Cu(1)−N(8) diminishes by 0.037 Å. Although more moderate, similar changes occur around the trigonal Cu(2) site; however, they are still significant with respect to the changes observed for the Fe^{II} site. From these facts, it would be more sensible to infer that the observed temperature-dependent structural changes at Cu sites are the driving force that provokes the residual spin-state change in Fe^{II} and not the contrary.

For temperatures above ca. 310 K, the fast increase of χ_MT corresponds to the mentioned irreversible spin transition ending around 360 K with a critical temperature T_c = 356 K. Once the system has reached ca. 390 K, new warming−cooling cycles reproduce a different and asymmetric SCO behavior with T_c = 187 K. This value is ca. 170 K smaller than that of the irreversible transition. This type of behavior has been observed in SCO materials when a new phase is generated as a consequence of the loss of solvent molecules; however, this cannot be the case for **1** because it is not a solvate. Another possibility could be the occurrence of an irreversible structural phase transition. Crystal structure determinations at 293 K, once the irreversible spin transition is surpassed, demonstrate that no crystallographic phase transition occurs in **1**. The most remarkable modification with respect to the structure determined at 293 K before the irreversible spin transition, as expected, corresponds to an increase of the average Fe−N bond lengths consistent with ca. 75% of Fe atoms in the HS state. Furthermore, the angles of the Fe−N(3)-C(11) and Fe−N(6)-C(14) moieties decrease 4.3° and 3.6°, respectively. It is worth noting that again the Cu(1) and Cu(2) sites demonstrate certain degrees of flexiblility. For instance, Cu(1)−N(7) and Cu(1)−N(8) distances increase by 0.018 and 0.019 Å, while Cu(1)−C(11) and Cu(1)−C(12) decrease by 0.015 and 0.011 Å, respectively. Similar bond variations are observed for Cu(2). At the same time, Cu(1) and Cu(2) experience strong angle variations; in particular, C(13)−Cu(2)−N(9) and C(14)−Cu(2)−N(9) deserve to be noted. The former decreases 5°, while the latter increases 6.1°. As indicated above, it is difficult to ascertain if the structural changes observed in the coordination sphere of the Cu sites in **1** are coupled to spin transition or to some extent are due to temperature-induced flexibility and hence to a low degree of crystal rigidity. The latter possibility is supported by the variation of the unit cell

(23) (a) Carlucci, L.; Ciani, G.; Macchi, P.; Proserpio, D. M. *Chem. Commun.* **1998**, 1837. (b) O'Keeffe, M.; Eddaoudi, M.; Li, H.; Reineke, T.; Yaghi, O. M. *J. Solid State Chem.* **2000**, *152*, 3.

volume, ΔV, which decreases ca. 67 Å^3 involving only 11% of Fe atoms when cooling from 293 to 130 K. This corresponds to ca. 17 Å^3 per Fe and represents approximately 50% of the volume variation found for a typical complete iron(II) spin transition. Between 130 K and 293 K*, ΔV changes 202.8 or 50.7 Å^3 per Fe. From this data, a value of ca. 68 Å^3 per Fe is extrapolated for 100% of spin conversion. This value doubles the ΔV typically found for an Fe^{II} SCO compound and confirms the high flexibility of framework **1**.

Concerning the magnetic behavior of **2**, the observation of two different slopes in $\chi_M T$ vs T suggests the occurrence of a not well-defined, two-step spin transition. This observation correlates well with the structural data because two slightly different Fe sites, Fe(1) and Fe(2), are observed. The average Fe−N bond length for site Fe(2) is 0.021 Å longer than that for site Fe(1) at 293 K, indicating the occurrence of a ligand field strength of ca. 6% stronger for site Fe(1). Compound **2** also presents a notable $\Delta V = V(360\ \text{K}) - V(140\ \text{K}) = 3123.1(2) - 2887.02(13) = 236.08$ or 59.02 Å^3 per Fe. In this case, although changes in the bond lengths and angles around the Cu sites are slightly smaller than those in **1**, the 3D nature of the network with NbO topology could also play a role because the Fe−N bond changes of ca. 0.18 Å per Fe can propagate more efficiently in the three directions of the crystal, affording a larger ΔV and compensating for the moderate changes observed in the Cu sites. It is interesting to note that a relatively large volume variation per Fe, $\Delta V = V(293\ \text{K}) - V(130\ \text{K}) = 46.2$ Å^3, has also been reported for the 1D system $\{Fe(3\text{-}CNpy)_2[Cu(3\text{-}CNpy)(CN)_2]_2\}$. This volume variation was considered essentially to arise from the significant change that occurred in the interchain Cu···Cu contacts [0.045(3) Å]. These examples contrast with the small volume variation, $\Delta V = V(293\ \text{K}) - V(90\ \text{K}) = 21.81$ Å^3, found for the 2D system $\{Fe(pyrimidine)_2[Cu(CN)_2]_2\}$. The more rigid structure of this compound is reflected in the Cu···Cu intermetallic interactions that change much less (0.014 Å) than those in the case of the 1D 3-CNpy system. This probably is the cause of the cooperative spin-transition behavior, accompanied by a hysteresis loop of 7 K, which strongly contrasts with the continuous spin transitions observed for **1**, **2**, and 3-CNpy derivatives.

Acknowledgment. This work was supported by the Spanish Ministerio de Educación y Ciencia (MEC) (Grant CTQ 2007-64727) FEDER and the European Network of excellence MAGMANET (Contract NMP3-CT-2005-515767-2). A.B.G. thanks the Spanish MEC for a research contract (Programa Ramón y Cajal).

Supporting Information Available: Magnetic behavior of **4** and **5** and CIF files of **1** (130 and 293 K and 293 K after warming at 360 K), **2** (140, 293, and 360 K), and **3**−**5** (293 K). This material is available free of charge via the Internet at http://pubs.acs.org.

IC8010458